New Journal of Physics
The open-access journal for physics

Two-fold origin of the deformation-induced ferromagnetism in bulk $Fe_{60}Al_{40}$ (at.%) alloys

E Menéndez[1], J Sort[2,5], M O Liedke[3], J Fassbender[3], S Suriñach[1], M D Baró[1] and J Nogués[4]

[1] Departament de Física, Universitat Autònoma de Barcelona, 08193 Bellaterra, Spain
[2] Institució Catalana de Recerca i Estudis Avançats (ICREA) and Departament de Física, Universitat Autònoma de Barcelona, 08193 Bellaterra, Spain
[3] Institute of Ion Beam Physics and Materials Research, Forschungszentrum Dresden-Rossendorf, PO Box 510119, D-01314 Dresden, Germany
[4] Institució Catalana de Recerca i Estudis Avançats (ICREA) and Institut Català de Nanotecnologia, Edifici CM7, Campus Universitat Autònoma de Barcelona, 08193 Bellaterra, Spain
E-mail: jordi.sort@uab.es

New Journal of Physics **10** (2008) 103030 (10pp)
Received 13 June 2008
Published 31 October 2008
Online at http://www.njp.org/
doi:10.1088/1367-2630/10/10/103030

Abstract. The transition from the atomically ordered B2-phase to the chemically disordered A2-phase and the concomitant deformation-induced ferromagnetism have been investigated in bulk polycrystalline $Fe_{60}Al_{40}$ (at.%) alloys subjected to compression processes. A detailed correlation between structural, magnetic and mechanical properties reveals that the generated ferromagnetism depends on the stress level but is virtually independent of the loading rate. The mechanisms governing the induced ferromagnetism also vary as the stress level is increased. Namely, in the low-stress regime both lattice cell expansion and atomic intermixing play a role in the induced ferromagnetic behavior. Conversely, lattice expansion seems to become the main mechanism contributing to the generated ferromagnetism in the high-stress regime. Furthermore, a correlation is also observed between the order–disorder transition and the mechanical hardness. Hence, a combination of magnetic and mechanical measurements can be used, in synergetic manner, to investigate this deformation-induced phase transition.

[5] Author to whom any correspondence should be addressed.

Contents

1. Introduction

Transition metal (TM) intermetallics exhibit outstanding functional properties, both from magnetic (e.g. soft FeNi alloys or hard $SmCo_5$ alloys) [1] and structural (e.g. low-density, high-strength TM aluminides, which also show good corrosion resistance) [2] points of view. In the case of the $Fe_{1-x}Al_x$ system, the room temperature magnetic moment of the atomically ordered alloy decreases slowly with increasing Al content, in agreement with dilution models, up to $x = 0.2$. With further dilution, the magnetic moment decreases more rapidly, becoming zero for alloys with $x \geqslant 0.32$. Remarkably, atomically ordered $Fe_{1-x}Al_x$ alloys with $x > 0.32$ can become ferromagnetic, at room temperature, after being disordered (i.e. atomically intermixed) [3]. The transition from the paramagnetic, chemically ordered, B2-phase to the ferromagnetic, chemically disordered, A2-phase in FeAl alloys can be accomplished by means of several techniques capable of inducing atomic intermixing, such as cold working procedures [4]–[8], ball milling, mechanical alloying [9]–[11] and ion irradiation [12]. From a theoretical basis, the ferromagnetism of diluted and disordered TM alloys has been explained by the so-called local environment model [13]–[15], which takes into account that the magnetic moment of a given atom (e.g. Fe) depends on the number of nearest-neighbor atoms of the same species. Using this simple model, the effect of Al substitution and disorder in, e.g., FeAl, can be qualitatively explained. However, since variations in the distance between TM atoms have profound effects on the magnetism, it is actually argued that the origin of the magnetic interactions in disordered TM alloys may not arise solely from nearest-neighbor magnetism (i.e. local environment model), but also from changes in the band structure of the material induced by changes in the lattice cell parameter (Δa) [9]–[11], [16]–[19]. Although the two-fold origin of the magnetism in FeAl alloys has been demonstrated for nanostructured materials [8], there are no studies of this effect on bulk samples.

In this paper, we report on the deformation-induced ferromagnetism in bulk polycrystalline $Fe_{60}Al_{40}$ (at.%) achieved by means of uniaxial compression tests performed at quasi-static conditions. A detailed correlation between structural (i.e. lattice cell parameter, crystallite size, microstrain and atomic intermixing), magnetic (i.e. M_S) and mechanical (i.e. microhardness) properties has been carried out by means of x-ray diffraction (XRD), Vickers microhardness and magnetometry. The origin of the ferromagnetism is found to be different for the

low-stress and high-stress regimes. Namely, in the low-stress testing range, both lattice cell expansion and atomic intermixing phenomena contribute to the amount of induced ferromagnetism. Conversely, at sufficiently high stresses, the induced ferromagnetism is mainly found to stem from lattice cell expansion. Interestingly, mechanical hardness correlates to some extent with this phase transition since both mechanical and magnetic hardening occur concurrently. Furthermore, virtually no influence of loading rate processing on the overall induced ferromagnetism has been detected.

2. Experimental

Gas-atomized $Fe_{60}Al_{40}$ (at.%) powders were pressure-less sintered at 1150 °C during 30 min of isothermal holding, in a tubular furnace under vacuum (air pressure $<10^{-5}$ mbar), in order to produce bulk specimens. The heating and cooling rates were chosen to be 5 °C min^{-1} in order to promote the sintering process. Note that since the employed processing temperature is below any transition temperature of the FeAl binary system [20], the process can be considered as solid-state sintering. Subsequently, cubic-shaped specimens (8 mm^3 volume) were cut and polished from two opposite sides up to mirror-like appearance, with the aim of obtaining parallel faces. Since both cutting and polishing steps already induce disorder (and thus ferromagnetism), the samples were annealed for 30 min at 650 °C in order to remove these ferromagnetic contributions, taking advantage of the annealing-induced, atomic reordering processes which recover the non-ferromagnetic state.

The compression processes were performed uniaxially at room temperature using a MTS 858 Table Top System Universal/Tensile apparatus, a loading rate of 1 kN s^{-1} and a dwell time of 100 s. Different engineering stresses were studied: 0.5, 2, 3, 4, 6 and 8 GPa. In addition, in order to investigate the loading rate influence on the induced magnetic properties, additional compression tests were also carried out at 0.1 kN s^{-1}.

The overall microstructural parameters, such as lattice cell parameters (a), crystallite sizes ($\langle D\rangle$, average coherently diffracting domain sizes), microstrains ($\langle\varepsilon^2\rangle^{1/2}$, atomic level deformations) and anti-site probabilities of Fe atoms at the Al positions (w_{Fe}, i.e. fraction of Al lattice sites occupied by Fe atoms) were evaluated by fitting the full XRD patterns (i.e. x-ray line profile analysis), recorded with Cu K_α radiation using a Philips X'Pert diffractometer, by means of the Rietveld refinement program MAUD (materials analysis using diffraction) [21]–[24]. The Vickers microhardness of the bulk samples was determined using a load of 0.1 kg ($H_{V0.1}$) by means of an FV700 indenter (Future-Tech). Finally, the magnetic characterization was performed at room temperature by means of a vibrating sample magnetometer (VSM, Oxford Instruments 1.2) with a maximum applied magnetic field of 1.1 T. The saturation magnetization was calculated from a least-squares fitting of the initial magnetization curves to the classical law of approach to saturation:

$$M = M_S\left(1 - \frac{a}{H} - \frac{b}{H^2}\right) + \chi H,$$

where H is the applied magnetic field, M_S is the saturation magnetization, χ is the field independent susceptibility and a and b are the coefficients which depend on the magnetic properties of the material [25].

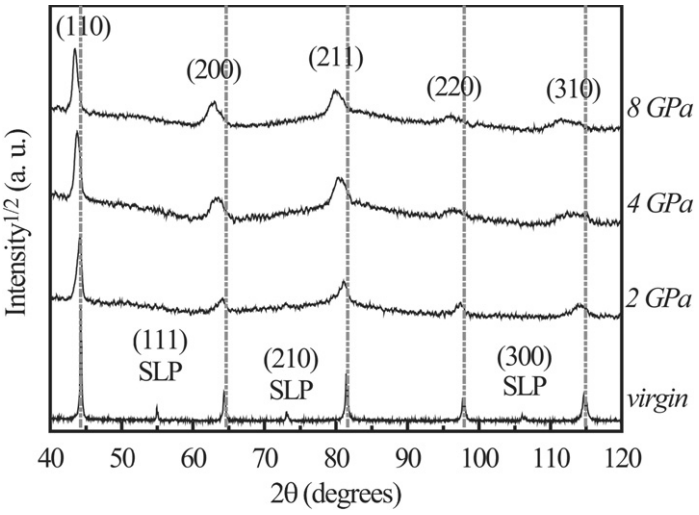

Figure 1. XRD patterns of the as-annealed $Fe_{60}Al_{40}$ (at.%) sample and the bulk specimens compressed uniaxially up to 2, 4 and 8 GPa using a loading rate of 1 kN s^{-1} and a dwell time of 100 s. The Miller indices of the different peaks have also been indicated in the figure. Note that SLP denotes super-lattice peaks.

3. Results and discussion

3.1. Structural characterization

The XRD patterns of the as-annealed $Fe_{60}Al_{40}$ (at.%) sample and the bulk specimens compressed up to 2, 4 and 8 GPa (using a loading rate of 1 kN s^{-1} and a dwell time of 100 s) are shown in figure 1.

The virgin sample (i.e. as-annealed) exhibits an XRD spectrum consistent with an atomically ordered BCC lattice structure (i.e. B2-phase). Conversely, for the pressed samples (applied engineering stress $\geqslant$3 GPa), super-lattice XRD peaks—denoted as SLP—vanish (see figure 1), evidencing that a severe atomic disordering process occurred upon deformation (i.e. leading to the so-called A2-phase). Nevertheless, for the mildest conditions (i.e. 0.5—not shown—and 2 GPa), some traces of the SLP peaks are still detectable (e.g. see the (210) super-lattice peak, located at $2\theta \approx 73^\circ$, corresponding to the sample compressed at 2 GPa), indicating that a less intense atomic intermixing (i.e. disordering) process occurred. Since the intensity of the SLP XRD peaks is linked to the atomic intermixing, x-ray line profile analysis allows assessing to some extent this order–disorder transition. Actually, since systems that exhibit order–disorder transitions (e.g. FeAl alloys) may exist in intermediate states, the degree of ordering becomes an essential physical property to characterize this type of system. The so-called long-range order (LRO) parameter can be defined as follows:

$$\mathrm{LRO} = \frac{x_{\mathrm{Fe}} - w_{\mathrm{Fe}}}{y_{\mathrm{Fe}}},$$

where x_{Fe} is the atomic concentration of iron ($Fe_{60}Al_{40}$ at.% $\Rightarrow x_{\mathrm{Fe}} = 0.6$), w_{Fe} is the anti-site probability of Fe atoms at the Al sites (which can be estimated by x-ray line profile analysis) and y_{Fe} is the iron-site probability (for a B2 structure it is equal to 0.5). For the $Fe_{60}Al_{40}$ stoichiometry, a totally ordered alloy results in LRO $\rightarrow$ 0.8, whereas for a completely atomically

Table 1. Lattice cell parameters, a, LRO parameters, crystallite sizes, $\langle D \rangle$, microstrains, $\langle \varepsilon^2 \rangle^{1/2}$, saturation magnetization, M_S, and microhardness, $H_{V0.1}$, of the as-annealed sample and the uniaxially compressed specimens up to 0.5, 2, 3, 4, 6 and 8 GPa using a loading rate of 1 kN s^{-1} and a dwell time of 100 s.

Engineering stress (GPa)	a ($\pm 5 \times 10^{-4}$ Å)	LRO (± 0.05)	$\langle D \rangle$ (± 5 nm)	$\langle \varepsilon^2 \rangle^{1/2} \times 10^{-3}$ (± 0.5)	M_S (± 2 emu g^{-1})	$H_{V0.1}$ (GPa)
0 (virgin)	2.8943	0.70	>200	<0.5	<2	2.9 ± 0.2
0.5	2.8947	0.52	165	1.1	<2	3.2 ± 0.2
2	2.9118	0.38	120	6.1	8	5.0 ± 0.3
3	2.9195	0.22	101	8.9	21	6.4 ± 0.3
4	2.9250	0.21	96	8.5	46	7.3 ± 0.3
6	2.9325	0.23	86	8.2	55	7.6 ± 0.3
8	2.9329	0.20	85	8.7	65	7.6 ± 0.3

disordered structure, LRO $\rightarrow$ 0 [26]–[28]. Thus, the degree of ordering increases as the anti-site probability of Fe atoms at the Al sites decreases.

From the x-ray line profile analysis, it can be inferred that a highly ordered structure is obtained for the as-annealed sample ($w_{Fe} \rightarrow 0.25$, thus LRO $\rightarrow$ 0.70), whereas a nearly fully disordered state is already attained for samples tested at $\geqslant$3 GPa ($w_{Fe} \rightarrow 0.50$, thus LRO $\rightarrow$ 0.20). However, intermediate states are achieved for specimens tested at 0.5 and 2 GPa ($w_{Fe} \rightarrow 0.34$, thus LRO $\rightarrow$ 0.52 and $w_{Fe} \rightarrow 0.41$, therefore LRO $\rightarrow$ 0.38, respectively)—see table 1.

Therefore, two clear regimes can be identified: a low-stress regime where disorder is generated by the stress and a high-stress regime where disorder remains unchanged despite the increased stress. Nevertheless, given the limited penetration of the x-rays (a few microns) [29], the obtained LRO parameter values are to some extent upper limits since the surface might have suffered more plastic deformation than the inner parts.

As the applied engineering stress increases, a broadening of the XRD peaks is observed due to both crystallite size refinement and increase of microstrains (see both figure 1 and table 1), since the amount of plastic deformation increases with the applied stress. Interestingly, while the crystallite size decreases slightly with the applied stress, the microstrain increases considerably (see table 1). Similar to the LRO parameter, both tend to saturate for applied stress above 3 GPa.

As the applied engineering stress increases, the lattice cell parameter, a, expands—see table 1—up to $\Delta a/a$ values of around 1.3% for the sample pressed at 8 GPa. This phenomenon is clearly evidenced by the XRD peak shifts to lower scattering angles (i.e. larger lattice cell parameters) as the stress increases. Remarkably, in contrast with the LRO parameter, which remains rather constant for high-stress regime ($\geqslant$3 GPa), the lattice cell parameter exhibits a continuous increase.

3.2. Magnetic characterization

The dependence of the magnetization of the as-annealed sample on the applied magnetic field (see figure 2, inset) evidences clear paramagnetic behavior, confirming the existence of an atomically ordered structure (B2-phase).

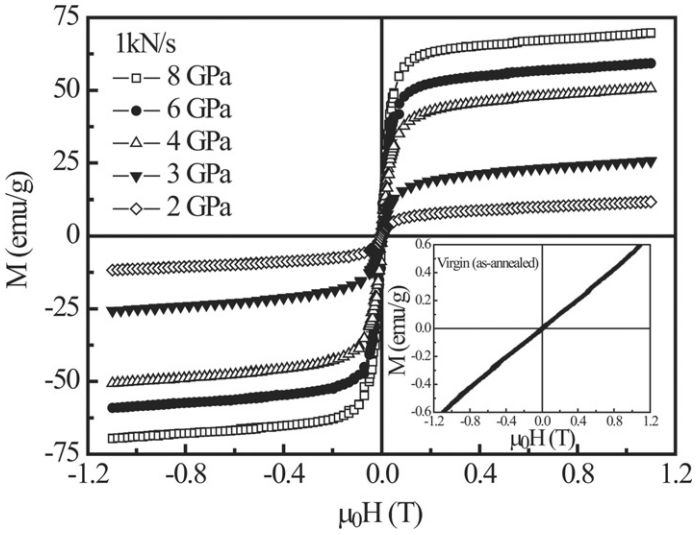

Figure 2. VSM measurements of the bulk $Fe_{60}Al_{40}$ (at.%) specimens compressed uniaxially up to 2, 3, 4, 6 and 8 GPa using a loading rate of 1 kN s^{-1} and a dwell time of 100 s. Shown in the inset is the VSM measurement of the as-annealed sample.

This is in agreement with previously reported results on annealed $Fe_{60}Al_{40}$ (at.%) powders, where the ordered B2-phase shows virtually no magnetization ($M_S < 0.2$ emu g^{-1}) [7, 10, 11]. In addition, the specimen compressed at 0.5 GPa also evidences no ferromagnetism (not shown). Conversely, the rest of the compressed samples show clear hysteretic behavior (see figure 2). The saturation magnetization, M_S, increases with the applied engineering stress (see table 1), thus confirming the increase of the ferromagnetic counterpart. The increase in M_S can be ascribed to the simultaneous increase of both atomic intermixing and lattice cell parameter [30]. However, when comparing LRO and M_S values (figure 3(a)), it can be observed that while the LRO already reaches a small constant value (disordered state) for tests carried out above 3 GPa, the ferromagnetism continuously increases up to 8 GPa.

Contrarily, in the high-stress regime, the lattice parameter continues to increase with higher stress in a way similar to M_S (see figure 3(b)). Consequently, these results demonstrate that the contribution from the lattice cell expansion to the ferromagnetic response seems to be significant, especially at the high applied stresses regime. Interestingly, although the contribution of the lattice expansion to the magnetism of FeAl alloys was proposed for ball-milled powders [10, 11], it was only confirmed through complex high pressure dichroism experiments [19]. Here, the two-fold origin of the ferromagnetic response of FeAl alloys is directly observed. Furthermore, the current experiments indicate that probably two regimes exist in the deformation-induced magnetism in these alloys. Note that due to the high strain rate conditions of ball milling, these two regimes were difficult to separate in our previous ball milling experiments [10].

According to the literature [19], the saturation magnetization of $Fe_{60}Al_{40}$ (at.%) powders in the A2-phase (with a parameter and a lattice cell spacing of LRO $= 0.14$ and $a = 2.9170$ Å—$\Delta a/a \approx 0.7\%$, respectively), achieved after long-term milling, is around 75 emu g^{-1} [10, 19]. Here, the obtained value of saturation magnetization for the sample pressed at 8 GPa is around 65 emu g^{-1} (highest value), even though greater lattice cell expansions are achieved in the

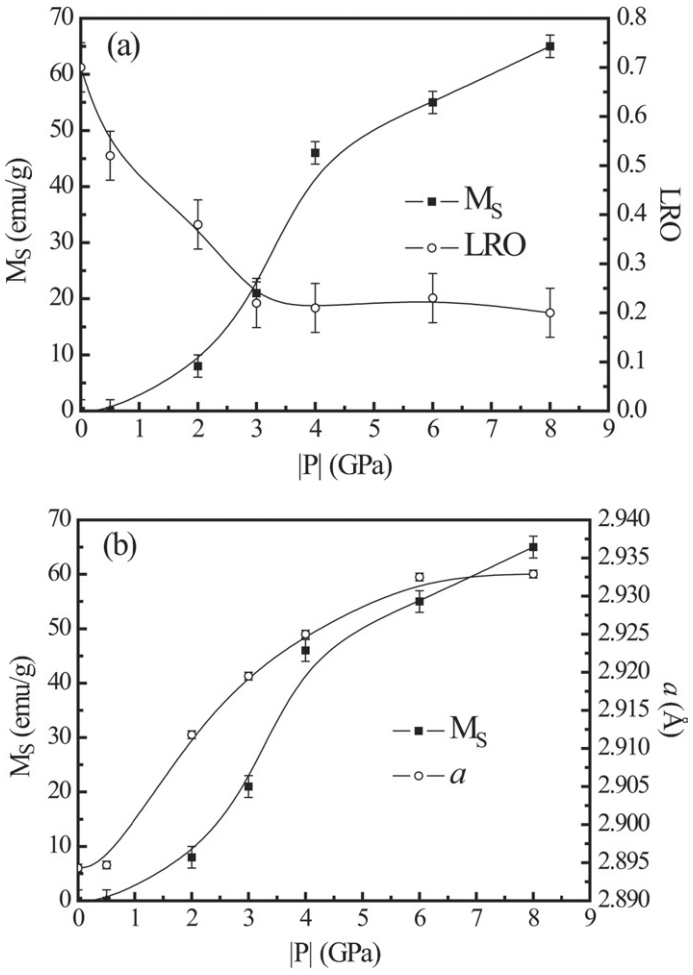

Figure 3. (a) Dependence of the saturation magnetization, M_S, and LRO parameter on the applied engineering stress $|P|$. (b) Dependence of M_S and the lattice cell parameter, a, on $|P|$. The lines are guides to the eye.

present investigation. This difference in the attained saturation magnetization values may be, to some extent, due to the fact that the obtained level of disorder is slightly lower than that reported in ball-milled samples, although a gradient of induced defects (i.e. more disorder at the surface) cannot be ruled out.

The possible influence of strain rate has also been investigated. Actually, strain rate is often one of the factors affecting the mechanical response of materials (e.g. the austenite (γ) to martensite (α') transformation in austenitic stainless steels) [31]. For this reason, compression tests at $0.1\,\mathrm{kN\,s^{-1}}$ were also performed and the resulting magnetic response investigated. As can be seen in figure 4, VSM measurements of specimens pressed at $0.1\,\mathrm{kN\,s^{-1}}$ render similar results to compression at $1\,\mathrm{kN\,s^{-1}}$, indicating that this order–disorder transformation is not especially sensitive to strain rate changes, at least within the assessed strain rate regime (i.e. quasi-static range).

However, in the dynamic (i.e. high strain rate range) regime (e.g. impact shock loading), differences have been observed when decreasing/increasing the strain rate. Namely, ball milling processes of $Fe_{60}Al_{40}$ (at.%) powders at higher milling intensities (i.e. larger angular

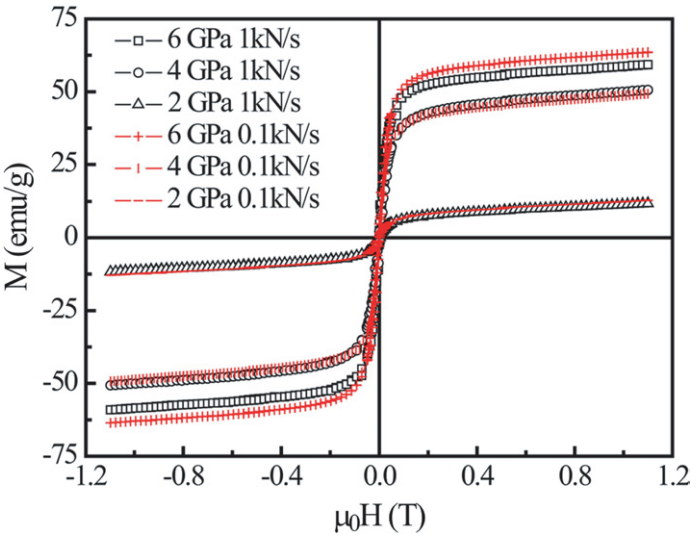

Figure 4. VSM measurements of the bulk $Fe_{60}Al_{40}$ (at.%) samples compressed uniaxially up to 2, 4 and 6 GPa using a loading rate of 0.1 kN s^{-1} (in red) and 1 kN s^{-1} (in black) and a dwell time of 100 s.

frequencies) lead to a larger ferromagnetic response [32]. Thus, since the deformation modes used in bulk (quasi-static) and ball milling powders (high strain rate) are different, the univocal comparison between the results of both types of specimens may be rather complex.

3.3. Mechanical hardness characterization

In FeAl alloys, plastic deformation causes simultaneously both a magnetic transformation and a mechanical hardening process [26, 32]. The mechanical hardness, measured by means of Vickers microhardness using a load of 0.1 kg, shows a progressive increase with the applied engineering stress from $H_{V0.1} = 2.9$ GPa (as-annealed sample) to $H_{V0.1} = 7.6$ GPa (specimen compressed at 8 GPa). Hence, the order–disorder transition can also be indirectly assessed by hardness measurements. In fact, there is a pronounced microhardness increase for low-stress range followed by steady-state-like behavior. Hence, the hardening effect is particularly significant for low processing stresses. Interestingly, as can be seen in figure 5, the $H_{V0.1}$ versus $|P|$ and M_S versus $|P|$ curves show similar trends during compression tests. A similar trend but opposite to that observed in LRO analysis (i.e. a prominent initial increase followed by a steady state) is noticed.

Several processes are responsible for the mechanical hardening phenomena. Actually, it is known that disorder-solution processes (i.e. solution of anti-sites in the ordered matrix) play an important role in hardening. Nevertheless, other structural effects (vacancy, dislocation or grain refinement) could also contribute to some extent to the aforementioned mechanical hardening [33]–[35].

4. Conclusions

In summary, the macro-scale deformation-induced ferromagnetism achieved by means of uniaxial compression tests performed at quasi-static conditions has been investigated in bulk paramagnetic $Fe_{60}Al_{40}$ (at.%) alloys. The correlation between structural (e.g. lattice cell

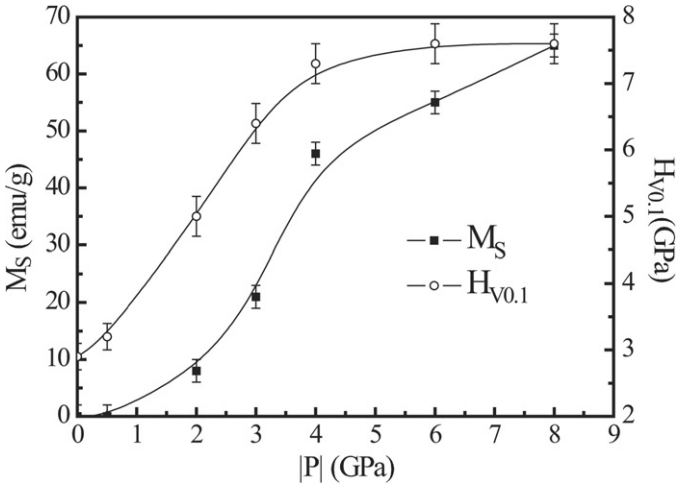

Figure 5. Dependence of the induced saturation magnetization, M_S, and the microhardness, $H_{V0.1}$, on the applied engineering stress, $|P|$. The lines are guides to the eye.

parameter, atomic intermixing, etc), magnetic and mechanical (microhardness) properties, indicates that the induced ferromagnetism is mainly controlled by both lattice cell expansion and atomic intermixing at low-stress-range processing. Conversely, lattice expansion seems to become the most important cause of the ferromagnetic response at the high-stress regime. Moreover, no influence of the loading rate on the induced ferromagnetism has been observed. Interestingly, the mechanical hardness characterization allows indirect assessment of this phase transition.

Acknowledgments

Partial financial support from 2005SGR-00401, PNL2006-019, MAT2007-66302-C02 and MAT2007-61629 research projects and the Institut Català de Nanotecnologia (ICN) are acknowledged. In addition, support by the EU-RITA program 'Center for the Application of Ion Beams in Materials Research' under contract no. 025646 is acknowledged. EM acknowledges his FPI fellowship from the Spanish Ministerio de Educación y Ciencia, co-financed by the ESF and S Enzo for useful discussions.

References

[1] Westbrook J H and Fleischer R L (ed) 2000 *Properties and Applications of Intermetallic Compounds: Magnetic, Electrical and Optical* vol 4 (New York: Wiley)
[2] Westbrook J H and Fleischer R L (ed) 2000 *Properties and Applications of Intermetallic Compounds: Structural Applications* vol 3 (New York: Wiley)
[3] Taylor A and Jones R M 1958 *J. Phys. Chem. Solids* **6** 16
[4] Varin R A, Czujko T, Bystrzycki J and Calka A 2002 *Mater. Sci. Eng.* A **329** 213
[5] Sort J, Concustell A, Menéndez E, Suriñach S, Rao K V, Deevi S C, Baró M D and Nogués J 2006 *Adv. Mater.* **18** 1717
[6] Huffman G P and Fisher R M 1967 *J. Appl. Phys.* **38** 735

[7] Yang Y, Baker I and Martin P 1999 *Phil. Mag.* B **79** 449
[8] Jirásková Y, Schneeweiss O, Milicka K, Svoboda M and Procházka I 2000 *Mater. Sci. Eng.* A **293** 215
[9] Yelsukov E P, Voronina E V and Barinov V A 1992 *J. Magn. Magn. Mater.* **115** 271
[10] Amils X, Nogués J, Suriñach S, Baró M D and Muñoz J S 1998 *IEEE Trans. Magn.* **34** 1129
[11] Hernando A, Amils X, Nogués J, Suriñach S, Baró M D and Ibarra M R 1998 *Phys. Rev.* B **58** R11864
[12] Fassbender J, Liedke M O, Strache T, Möller W, Menéndez E, Sort J, Rao K V, Deevi S C and Nogués J 2008 *Phys. Rev.* B **77** 174430
[13] Beck P A 1971 *Metall. Trans.* **2** 2015
[14] Wertheim G K, Jaccarino V, Wernick J H and Buchanan D N E 1964 *Phys. Rev. Lett.* **12** 24
[15] Takahashi S 1986 *J. Magn. Magn. Mater.* **54–57** 1065
[16] Fujii M, Saito K, Wakayama K, Kawasaki M, Yoshioka T, Isshiki T, Nishio N and Shiojiri M 1999 *Phil. Mag.* A **79** 2013
[17] Smirnov A V, Shelton W A and Johnson D D 2005 *Phys. Rev.* B **71** 064408
[18] Apiñaniz E, Plazaola F and Garitaonandia J S 2003 *Eur. Phys. J.* B **31** 167
[19] Nogués J *et al* 2006 *Phys. Rev.* B **74** 024407
[20] Massalski T B 1987 *Binary Alloy Phase Diagrams* ed J L Murray, L H Bennett and H Baker (Ohio: American Society for Metals)
[21] Young R A 1995 *The Rietveld Method* (Oxford: International Union of Crystallography, University Press)
[22] Warren B E and Averbach B L 1950 *J. Appl. Phys.* **21** 595
[23] Lutterotti L and Scardi P 1990 *J. Appl. Crystallogr.* **23** 246
[24] Enzo S, Fagherazzi G, Benedetti A and Polizzi S 1988 *J. Appl. Crystallogr.* **21** 536
[25] Chikazumi S 1964 *Physics of Magnetism* (New York: Wiley) p 277
[26] Amils X, Nogués J, Suriñach S, Muñoz J S, Lutterotti L, Gialanella S and Baró M D 1999 *Nanostruct. Mater.* **11** 689
[27] Gialanella S, Amils X, Baró M D, Delcroix P, Le Caër G, Lutterotti L and Suriñach S 1998 *Acta Mater.* **46** 3305
[28] Morris D G, Amils X, Nogués J, Suriñach S, Baró M D and Muñoz-Morris M A 2002 *Int. J. Non-Equilib. Process.* **11** 379
[29] Cullity B D 1978 *Elements of X-Ray Diffraction* (Boston, MA: Addison-Wesley)
[30] Apiñaniz E, Plazaola F and Garitaonandia J S 2004 *J. Magn. Magn. Mater.* **272–276** 794
[31] Dieter E 1988 *Mechanical Metallurgy* (London: McGraw-Hill)
[32] Amils X, Nogués J, Suriñach S, Muñoz J S, Lutterotti L and Baró M D 1999 *Nanostruct. Mater.* **12** 801
[33] Meyers M A, Mishra A and Benson D J 2006 *Prog. Mater. Sci.* **51** 427
[34] Yang Y and Baker I 1998 *Intermetallics* **6** 167
[35] Amils X, Nogués J, Suriñach S, Baró M D, Morris-Muñoz M A and Morris D G 2000 *Intermetallics* **8** 805